Materials Research. 2023; 26:e20230227
DOI: https://doi.org/10.1590/1980-5373-MR-2023-0227

Dielectric Anomaly Origin Study for Ferroelectric Ceramic of Type PZT52/48 Erbium-doped at High-temperatures

***Jaime Alberto Sanchez Caceres*[a]*, *Carlos Augusto Cardoso Passos*[a]**

[a]*Universidade Federal do Espírito Santo, Vitória, ES, Brasil.*

Received: May 05, 2023; Revised: September 30, 2023; Accepted: October 20, 2023

In present work, erbium-doped PZT 52/48 ceramics at sites A and B were prepared by the Pechini method in order to study their dielectric properties. The aim was investigated the dielectric anomalies of interfacial origin in these ferroelectrics. The ceramics were also submitted to electrical measurement analysis. The dielectric response of the grains showed characteristics of materials that follow Curie-Weiss law which is typical of ferroelectrics. In high temperatures and low frequencies, it was detected the dielectric anomaly phenomenon for the ceramic samples. Impedance spectroscopy analyzes through equivalent circuit (brick-layer model), grain and grain boundary in series, exposed a predominance of dielectric properties of intergranular interfaces as the cause of this anomaly. The electrical characterization showed a peculiar ferroelectric-paraelectric phase transition around 390 °C for both samples.

Keywords*: PZT-based, Impedance spectroscopy, Dielectric properties, Dielectric anomalies.*

1. Introduction

The lead zirconate titanate solid solutions, $Pb(Zr_{1-x}Ti_x)O_3$, are widely recognized to represent a special group of perovskite-type $A(B'B'')O_3$ ferroelectric materials[1]. It is classified as ABO_3 perovskite family, being A a divalent cation (Pb^{+2}) and occupies at corners of the cube, B is a tetravalent cation (Zr^{+4} orTi^{+4}) occupies at body centered position and "O" is the oxygen atoms at the face centered positions of the cubic structure. Consequently, there are wide variety of cations to form a perovskite structure. From the parent structure, it can obtain other structures using the Goldschmidt factor (tolerance factor) $t = \frac{R_A + R_O}{\sqrt{2}\left(R_B + R_O\right)}$[1].

Where R_A (Pb^{+2}), R_B (Zr^{+3} or Ti^{+3}), and R_O (O^{-2}) are the ionic radius of the large cation, the small cation, and the oxygen ion, respectively[1]. This ABO_3 perovskite can present ferroelectric (F) and antiferroelectric (AF) characteristics. If t is in the range of 0.95 to 1.00, the perovskite has cubic crystalline structure, for $t < 0.95$, the compound does not appear the antiferroelectric property, and $t > 1.00$ the perovskite material has ferroelectric. However, pure PZT material has poor dielectric, ferroelectric, piezoelectric properties which is a drawback for technological applications. On the other hand, the properties of PZT can be tuned by doping with donor dopants like Nb^{+5}, Sb^{+}, and Ta^{+5}, or lanthanide ions Ln^{+3} (Ln = La, Nd, Sm, Gd, Dy, Ho, Er, and Yb)[2]. In addition, dopants on either side the A site or the B site produce ferroelectric–antiferroelectric phase transition when tolerance factor is changed[1].

Basically, there are three types of dopants are used in the compositional modification of PZT material: isovalent dopants, donor dopants and acceptor dopants. Isovalent dopants are characterized by similar valence and ionic radii of the replaced ions[1,2]. This type of dopant causes a drop in the Curie temperature, the permittivity is enhanced, the loss factor is lower, and the aging rate is increased. The donor dopants are used with higher valence cations and induce cation vacancy. The acceptor dopants are those cations with lower valence and induce oxygen vacancy[1,2].

The electrical properties of the PZT composites have become such system as an important technological application, for example, transducers, amplifiers, piezoelectric, pyroelectric, and ferroelectric memory sensors[3]. The high dielectric permittivity of ferroelectrics compounds immediately placed them as major candidate for manufacturing high quality capacitors[4,5]. In addition, these piezoelectric materials have induced an accelerated development in the field of detectors until today, sounders and transducers detectors until today. The demand for computers with high memory capacity has also made ferroelectrics a favorite material due to their bistable polarization, generating the potential for its use for binary memories (FRAM: Ferroelectric Random-Access Memories)[6].

In literature, it is well known that the sintering temperature of PZT compounds is in range of 1200 – 1300 °C, which causes a significant loss of PbO by volatilization. These isothermals require electrodes for multilayes system to noble metals, for instance, expensive platinum[5,7]. In addition, loss of PbO results in environmental pollution problems, causes breaking of the desired composition stoichiometry and deteriorates the ceramics properties. An alternative is to discover lead-free candidates with superior piezoelectricity as reported in references[7-12]. On the other hand, many chemical methods have been employed to achieve highly reactive powders with low compositional fluctuations[13-15]. And as consequence, the temperature of synthesis is lower and influence the density and microstructure which control the ceramic properties[14].

*e-mail: jcaceres.vix@gmail.com

A fundamental characteristic of ferroelectric materials is their permittivity which is well known to follow the permittivity versus temperature dependence and described by the Curie-Weiss law. However, the literature reports several cases in which compliance with this law is not verified, which has been called a dielectric anomaly, and includes the possible occurrence of non-electrical dielectric peaks associated with iron-paraelectric transitions in these materials[3,15,16]. In general, the investigation of the origin of dielectric anomalies in ferroelectric materials sometimes is evaluated by impedance spectroscopy. Such a non-destructive technique can identify and separate volumetric (grain) and interfacial (inter-grain and material-electrode) dielectric responses. In fact, the technique allows definitively distinguishing these micro-regions from interfaces since the ferroelectric properties of grains may be described by Curie-Weiss law.

In this context, the proposal of the present work is the study of the structural and dielectric properties of conventionally prepared Er-doped PZT ceramics having particularly the Zr/Ti = 52/48 composition out from the conventional MPB. In the present work, the influence of Er doping is closely considered.

2. Experimental

Our samples of the $(Pb_{1-x}Er_x)(Zr_{0.52}Ti_{0.48})O_3$ – PZT52/48 – solid solution were prepared in powder form. The preparation was performed considering the phase diagram in the interface region of the morphotropic phase of the two solid solutions $PbZrO_3$ (PZ) and $PbTiO_3$ (PT). The synthesis route to prepare the samples was by the polymer precursor method (Pechini method modified)[13,17]. The raw materials used were Lead Acetate $(PbCH_3COO)_2.3H_2O$ – Aldrich 99%), Titanium Isopropoxide $(Ti(OCH(CH_3)_2)_4$ – Alfa Aesar 97%), Zirconium Oxide Dinitrate $(ZrO(NO_3)_2.H2O$ Alfa Aesar 97%) where these reagents were weighted out in the desired molar ratios. The mixtures of these materials were dissolved in citric acid monohydrate ($C_6H_8O_7H_2O_2$ – Synth 99.5%) and an aqueous solution in constant stirring and heating approximately at 150 °C[13,17]. Finally, ethylene glycol ($C_2H_6O_2$ – Synth 99%) was added in a mass ratio of 40% ethylene glycol to 60% citric acid monohydrate. After that, each PZT precursor $(Pb_{1-x}Er_x(Zr_{0.52}Ti_{0.48})O_3)$ was added Erbium Oxide (Er_2O_3 – Alfa Aesar 99%) with x = 0.5 moles percent. From here we are designated as PZTA05 and PZTB05. Then the obtained resin was calcined at 400 °C to eliminate organic matter and at 700 °C to crystallize the precursor material. This last heat treatment resulted in precursors in powder form. The resultant powders were pelletized by using a uniaxial press 80 kgf/cm^2 for 20 s and then the samples were sintered at 895 °C and 845 °C determined through the dilatometry tests for PZT05A and PZT05B, respectively.

After sintering, the relative densities of samples were determined by the Archimedes' method. The densities were above 96% of its theoretical density. Finally, dielectric studies were realized using the impedance spectroscopy technique. The measurements were carried out with a Solartron SI 1260 impedance analyzer, to f = 1 MHz (f =ω/2π is the linear frequency), and from room temperature up to 550 °C. The entire process was computer controlled.

3. Results and Discussion

3.1. Ceramic dielectric characterization

The permittivity behavior of PZT-Er ceramics as a function of temperature at different frequencies (1 kHz, 10 kHz, 100 kHz and 1000 kHz) are displayed in Figure 1 for samples sintered. As can be noted, the maximum peak position (εm ≡ ε (*Tc*)) does not depend on if the substitution of the Er^{3+} ion either in site A or in site B. However, it is observed an increasing in the magnitude of dielectric constant above 420 °C at 1 kHz and from the 470 °C at 10 kHz. Both occur above the Curie temperature (*Tc*), that is, the permittivity increases above of *Tc* at low frequencies.

At low frequencies, it is also observed that the permittivity reaches values significantly higher than the εm, where there is a deviation from the expected linear trend for the Curie-Weiss law. This deviation from the linear tendency of the permittivity above the Curie temperature is the dielectric anomaly, which has also been reported by some authors in the literature for the same compound and other types of ferroelectric materials[18,19].

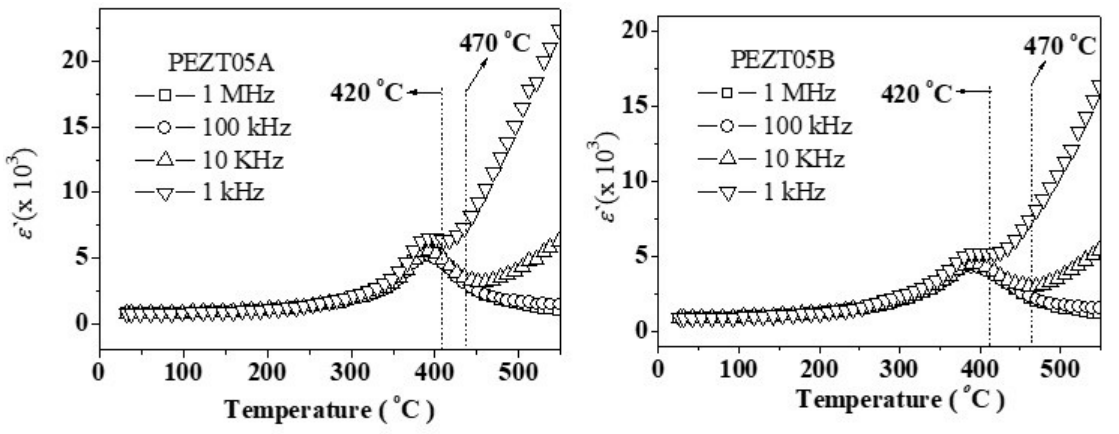

Figure 1. Dependence of permittivity with temperature according to measurements performed at various frequencies (from 1 kHz to 1 MHz) for the PEZT05A and PEZT05B samples.

In our point of view, the causes of dielectric anomalies in ferroelectric materials can be varied and are related to intrinsic or extrinsic origins: inter-grain and material-electrode interfaces, volumetric effects involving the combination of polarization and conduction processes, inductive effects, etc[20-23]. The dielectric properties of ferroelectric materials must be measured at high frequencies to extract their strictly ferroelectric characteristics over a wide range of temperatures, as the anomaly can reach significant relevance and make it difficult to evaluate parameters (such as permittivity, for example).

In Figure 2 and Figure 3 are shown the impedance spectra measured at two different temperatures (420 and 470 °C). Each point on the graphs corresponds to measurements performed at a given frequency. Note the occurrence of two semicircles assigned to the grain and to the grain boundary.

The equivalent electric circuit propose that this type of dielectric response suggests that the ceramic material (non-homogeneous in nature) can be represented by an RC circuit like the configuration described in Figure 4. In this figure, there are two R-C blocks, where each of the two resistor elements R and capacitor C (in each block) are coupled in parallel, while the two blocks are connected in series[24]. Each of these blocks is representative of a combined conduction process (in parallel) with polarization, being theoretically responsible for the occurrence of a semicircle in the complex impedance planes.

The complex impedance of the equivalent circuit can be described as (Equation 1):

$$Z^*(\omega) = Z' - j\,Z'' = \sum_i \left(\frac{R_i}{1+\omega^2\ \tau_{ci}^2} - j\ \frac{R_i\ \omega\ \tau_{ci}}{1+\omega^2\ \tau_{ci}^2} \right) \qquad (1)$$

where ***i*** represents the number of R-C blocks involved, and τ_c ($\equiv R$ x C) the relaxation time (or time constant) of each block.

The solid lines shown in Figure 2 and Figure 3 indicate the best fit with the experimental data points in order to obtain semicircles of resistivity related to grains and grain boundaries. The fitting was done with ZView software which contemplates the possibility of using constant phase elements (EFC – associated with the consideration of non-ideal capacitances) in place of ideal C capacitances[12].

It is important to point out that in this work, the capacitances exhibited values of the order of 10^{-10} F for the semicircles of high frequencies, and of the order of 10^{-8} F for those of low frequencies, which is in agreement with values found in commercial PZT ceramics, where they exhibit values on the order of 10^{-8} to $10^{-1018-22}$. Furthermore, those semicircles can be interpreted here due as grains at high frequencies and grain boundaries at low frequencies.

With these results, a visual and direct comparison between Figure 1, Figures 2 and 3 allows building a qualitative idea of the origin of the analysed dielectric anomaly. At a temperature of 420ºC, for example, while the frequency of 1 kHz is in the semicircle corresponding to the grain boundaries, the other frequencies above of 1kHz are at the semicircle of the grains (Figures 2 and 3). For temperature of 420ºC, the frequency of 1 kHz is in the region of occurrence of the dielectric anomaly, while the measured permittivity at other frequencies does not show deviation from the expected Curie-Weiss law (Figure 3). These analyses are summarized in Table 1 and Table 2.

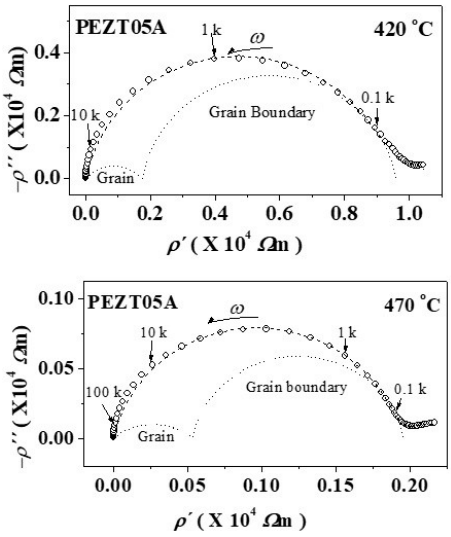

Figure 2. Nyquist Plots for the PEZT05A sample measured at 420 °C and 470 °C. The measurements were done nthefrequencyrange 0.1 kHz – 100 kHz to exhibit two semi-circular arcs due to bulk (grains) and grain boundary contributions in sequence.

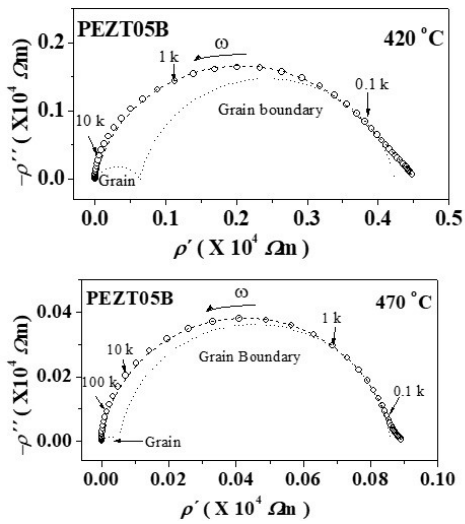

Figure 3. Nyquist Plots for the PEZT05B sample measured at 420 °C and 470 °C. The measurements were done in the frequency range 0.1 kHz – 100 kHz to exhibit two semi-circular arcs due to bulk (grains) and grain boundary contributions in sequence.

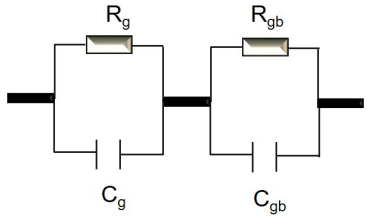

Figure 4. Equivalent circuit of the material according to the impedance spectra showing two semicircles in Figures 2 and 3. It consists of two R-C blocks connected in series where every two R and C elements are arranged in parallel.

Table 1. Location of some frequencies according to each semicircle (grain or grain boundaries) and region of compliance or not with the Curie-Weiss law (CWL) for some measurement temperatures in the case of the PEZT05A sample.

T (° C)	f (kHz)	Location according to the semicircle at the Figure 1	Observation according to Figure 2
420	1	Grain B.	CWL → No
	10, 100 e 1000	Grain	CWL → Yes
470	1 and 10	Grain B.	CWL → No
	100 e 1000	Grain	CWL → Yes

Table 2. Location of some frequencies according each semicircle (grain or grain boundaries) and region of compliance or not with the Curie-Weiss law (CWL) for some measurement temperatures in the case of the PEZT05B sample.

T (° C)	f (kHz)	Location according to the semicircle at the Figure 1	Observation according to Figure 3
420	1	Grain B.	CWL → No
	10, 100 and 1000	Grain	CWL → Yes
470	1 e 10	Grain B.	CWL → No
	100 and 1000	Grain	CWL → Yes

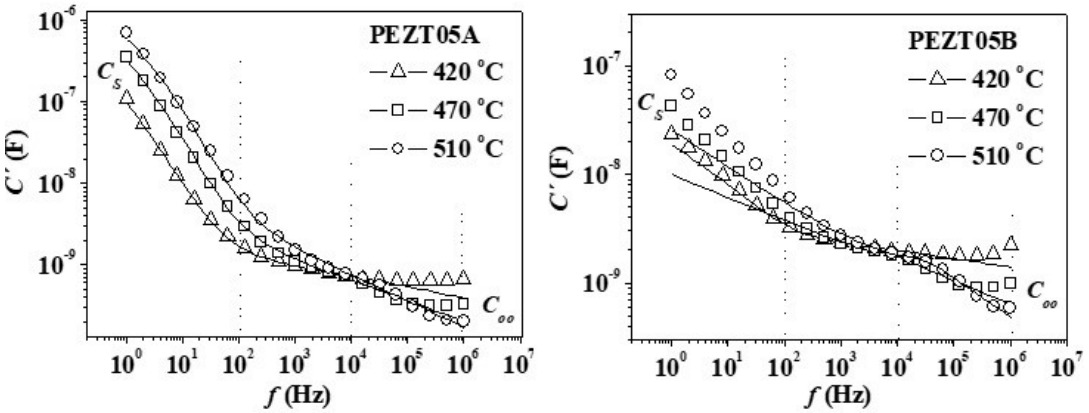

Figure 5. Frequency spectrum of the real part of the capacitance according to measurements performed at several temperatures for all sintered samples.

These observations allow us to conclude that the dielectric anomaly manifests itself when the dielectric response of the material starts to reflect and response corresponding to the grain boundaries. This is not necessarily the response of the material ferroelectric properties, which are essentially defined as volumetric. This interpretation is supported in references[20-23].

3.2. Dielectric anomaly: semi-quantitative correlation

An important question is that related to the level (in the sense of intensity) at which grain boundaries (or interfaces, in general) can disturb the ferroelectric response of materials. The issue is trying understood up to what levels of "abnormality" the permittivity is expected to increase by increasing the temperature above Tc (as shown in Figure 1).

The shape and the width of the arc indicate the type of relaxation mechanism for the system. In the present case depressed semi circles were observed indicating a distribution of the relaxation time. Our results suggest that model can use an ideal capacitor ($C^* = [j\ \omega Z^*]^{-1}$). And considering a series combination between grains (g) and grain boundaries (gb), the total capacitance[24] of the material must obey the relationship (Equation 2):

$$C^*(\omega) = C' - j\ C'' = \left[C_\infty + \frac{C_s - C_\infty}{1+\omega^2\ \tau_p^2} \right] - j \left[\frac{1}{\omega\ (R_g + R_{cg})} + \frac{(C_s - C_\infty)\ \omega\ \tau_p}{1+\omega^2\ \tau_p^2} \right] \quad (2)$$

where $C_s = \dfrac{C_g\ R_g^2 + C_{cg}\ R_{cg}^2}{(R_g + R_{cg})^2}$ and $C_\infty = \dfrac{C_g\ C_{cg}}{C_g + C_{cg}}$ represent regions of capacitance (the real part, in this case) independent of frequency in the direction, respectively, of the low and the high frequencies.

In Figure 5 it is shown the complete dielectric spectrum of the capacitance (real part) measured for the samples over a wide range of frequencies and at various temperatures. The continuous curves are simulations of the data performed from the equivalent circuit (Figure 4) using EFC-type capacitances.

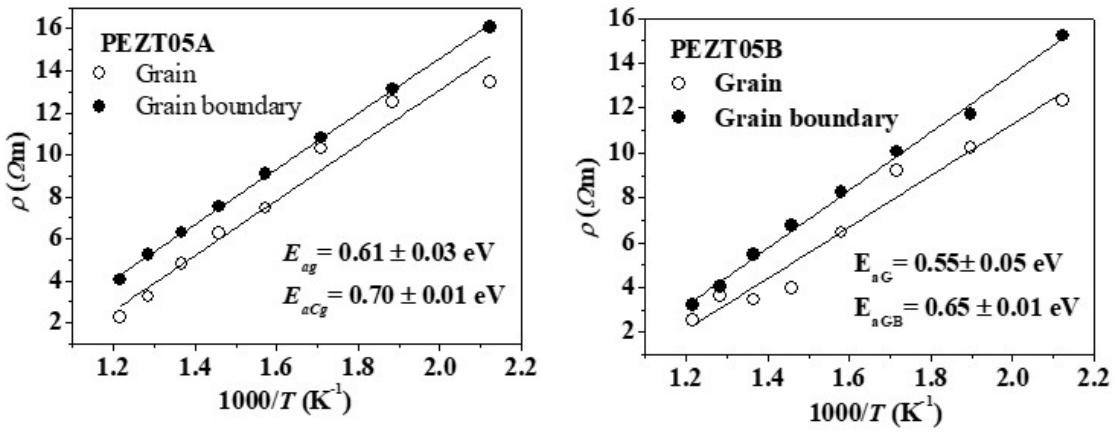

Figure 6. Arrhenius plot for resistivity of grains and grains boundaries for all ceramic samples.

Table 3. Values obtained for activation energies (ΔE), resistivities (ρ) and capacitances (*C*) at 420 ºC, according to the microstructural region of grains or grain boundaries at the PEZT samples.

Samples	ΔE (eV)		ρ (kΩm)		C (nF)	
	Grain	Grain B.	Grain	Grain B.	Grain	Grain B.
PZT	0.43	0.88	317	1540	0.42	3.2
PEZT05A	0.45	0.87	668	2400	0.22	2.8
PEZT05B	0.62	0.93	57	1600	0.11	4.2

A dispersion of the total capacitance of the material is observed moving from C_∞ at high frequencies, $C'(\omega\rightarrow\infty) = C_\infty$, and also for C_s at low frequencies, $C'(\omega\rightarrow 0) = C_s$ as indicated by the Equation 2. Any increase in capacitance is due to the additional polarization process, which is known as Maxell-Wagner interfacial polarization[24] and expresses itself with the relaxation time $\tau_p = \frac{R_g\ R_{cg}}{R_g + R_{cg}}\ (C_g + C_{cg})$.

To complete the analysis, Figure 6 illustratively shows the data obtained for the resistivity (ρ) of the grains and grain boundaries for all samples, according to the Arrhenius-type graphic. Linear behaviours are observed, and each data set can be described according to the equation of Arrhenius law (Equation 3):

$$R = R_o exp\ (-\Delta E / k\ T) \quad (3)$$

where R_o is the pre-exponential factor, ΔE the activation energy (or energy barrier) of the conductive processes involved, k the Boltzmann constant and T the absolute temperature. Table 3 shows the values obtained for ΔE, in addition to the resistivity and capacitance values at a certain measurement temperature (420ºC), for all the samples studied.

In particular, the values obtained for ΔE are agreement with the results of the literature for PZT-based ceramics involving processes of conduction by oxygen vacancies (acting as charge carriers)[25-30]. These values show to be higher for the grain boundaries in relation to the grains, indicating that the first region is relatively more resistive in relation to the second. The consequence of this relationship is that, during their migration process through the material, the charge carriers are partially accumulated at the grain boundaries. And it implies to give rise to an interfacial polarization (see Figure 5) that causes the dielectric anomaly. This corroborates to analysis of Figure 1.

4. Conclusions

Ferroelectric PZT ceramics were here studied, showing aspects such as high permittivity, observation of dielectric peaks denoting the ferroelectric-paraelectric phase transition and compliance with the Curie-Weiss law in a wide range of temperatures, the phenomenon of dielectric anomaly was observed at low frequencies and high temperatures. Under these conditions (of frequency and temperature), the anomaly revealed as a deviation from the material total permittivity data from the Curie-Weiss law. Considering the impedance spectroscopy via equivalent circuit (layers in series model, it was possible to establish that the dielectric anomaly is a consequence of the influence of the dielectric properties of the grain boundaries, whose dielectric responses are dominant at low frequencies.

5. Acknowledgments

The authors gratefully acknowledge academic supports and material support from CAPES, FAPES (Brazilian research-funding agencies) and the Institute of Physic of São Carlos, University of São Paulo.

6. References

1. Gonnard P, Troccaz M. Dopant distribution between A and B sites in the PZT ceramics of type ABO_3. J Solid State Chem. 1978;23:321-6.

2. Park H, Park CY, Hong Y, Kim K, Kim S. Structural and dielectric properties of PLZT ceramics modified with lanthanide ions. J Am Ceram Soc. 1999;82(1):94-102.
3. Zhang S, Xia R, Lebrun L, Anderson D, Shrout TR. Piezoelectric materials for high power, high temperature applications. Mater Lett. 2005;59(27):3471-5.
4. Jayakrishnan AR, Silva JPB, Kamakshi K, Dastan D, Annapureddy V, Pereira M, et al. Are lead-free relaxor ferroelectric materials the most promising candidates for energy storage capacitors? Prog Mater Sci. 2023;132:10104.
5. Qi J, Zhang M, Chen Y, Luo Z, Zhao P, Su H, et al. High-entropy assisted BaTiO3-based ceramic capacitors for energy storage. Cell Reports Physical Science. 2022;3(11):101110.
6. Sheikholeslami A, Gulak PG. A survey of circuit innovations in ferroelectric random-access memories. Proc IEEE. 2000;88:667-89.
7. Gao X, Jin H, Xin B, Wang M, Dong S, Xu Z, et al. Low temperature sintering of Li2CO3 added Pb(Ni1/3Nb2/3)-Pb(Zr,Ti)O3 ceramics with high piezoelectric properties. J Alloys Compd. 2022;892(5):162132.
8. Mazumder R, Sen A. Ultra-low-temperature sintering of PZT: a synergy of nano-powder synthesis and addition of a sintering aid. J Eur Ceram Soc. 2008;28(14):2731-7.
9. Cai W, Zhang Q, Zhou C, Gao R, Wang F, Chen G, et al. Effects of oxygen partial pressure on the electrical properties and phase transitions in (Ba,Ca)(Ti,Zr)O3 ceramics. J Mater Sci. 2020;55:9972-92.
10. Zeng F, Zhou C, Zhang C, Jiang L, Zhang J, Guo H, et al. Effects of Hf^{4+} substitute on the enhanced electrostrain properties of 0.7BiFeO3-0.3BaTiO3-based lead-free piezoelectric ceramics. Ceram Int. 2022;48(8):10539-46.
11. Rodel J, Jo W, Seifert KTP, Anton EM, Damjanovic D. Perspective on the development of lead-free piezoceramics. J Am Ceram Soc. 2009;92(6):1153-77.
12. Jo W, Dittmer R, Acosta M, Zang J, Groh C, Sapper E, et al. Giant electric-field-induced strains in lead-free ceramics for actuator applications – status and perspective. J Electroceram. 2012;29(1):71-93.
13. Abreu A Jr, Zanetti SM, Oliveira MAS, Thim GP. Effect of urea on lead zirconate titanate - Pb(Zr0.52Ti0.48)O3 - nanopowders synthesized by the Pechini method. J Eur Ceram Soc. 2005;25:743-8.
14. Wu H, Li W, Ao H, Zeng Z, Qin X, Xing S, et al. Effect of holding time on microstructure, ferroelectric and energy-storage properties of Pb0.925La0.05Zr0.95Ti0.05O3@SiO2 ceramics. J Alloys Compd. 2022;896:162932.
15. Li C, Xu R, Gao R, Wang Z, Chen G, Deng X, et al. Structure, dielectric, piezoelectric, antiferroelectric and magnetic properties of CoFe2O4–PbZr0.52Ti0.48O3 composite ceramics. Mater Chem Phys. 2020;249:123144.
16. Uchino K. Ferroelectric devices. 2nd ed. Boca Raton: CRC Press; 2009.
17. Pechini MU. Method of preparing lead and alkaline earth titanates and niobates and coating method using the same to form a capacitor. United States patent US 3330697. 1967, Jul 11.
18. Thong HC, Zhao C, Zhou Z, Wu C, Liu Y, Du Z, et al. Technology transfer of lead-free (K,Na)NbO3-based piezoelectric ceramics. Mater Today. 2019;29:37-48..
19. Lines ME, Glass AM. Principles and applications of ferroelectrics and related materials. Oxford: Oxford Univ. Press; 1977. (Oxford Classic Texts in the Physical Sciences).
20. Pilgrim SM, Sutherland AE, Winzer SR. Diffuseness as a useful parameter for relaxor ceramics. J Am Ceram Soc. 1990;73(10):3122-5.
21. Shannigrahi SR, Choudhary RNP, Acharya HN. X-ray, SEM and dielectric studies of Gd-modified sol–gel-prepared lead zirconate–lead titanate solid solution. Mater Lett. 1999;39(6):318-323.
22. Buchenan RC. Ceramic materials for electronics (3rd ed.). Boca Raton: CRC Press; 1986.
23. Delgado A, García-Sánchez MF, M'Peko J-C, Ruiz-Salvador AR, Rodríguez-Gattorno G, Echevarría Y, et al. An elementary picture of dielectric spectroscopy in solids: physical basis. J Chem Educ. 2003;80(9):1062-73.
24. Macdonald JR. Impedance spectroscopy: emphasizing in solid state materials and systems. New York: John Wiley; 1987. 346 p.
25. Caceres JAS, Passos CAC. Effect of Er ion substitution on the micro-structural and electrical properties using a polymeric precursor method in PZT52/48 ceramics. J Phys Chem Solids. 2022;160:110375.
26. Caceres JAS, Passos CAC. Electrical and ferroelectric properties of undoped and er-doped PZT52/48 electroceramics synthesized by a polymeric precursor method. Mater Res. 2021;25:20200538.
27. Koura P, Kumar P, Sinha SK, Kar M. Electrical properties of calcium modified PZT (52/48) ceramics. Solid State Commun. 2014;190:33-9.
28. Du Z, Zhao C, Thong H-C, Zhou Z, Zhou J, Wang K, et al. Effect of MnCO3 on the electrical properties of PZT-based piezoceramics sintered at low temperature. J Alloys Compd. 2019;801:27-32.
29. Han B, Zhao C, Zhu Z-X, Chen X, Han Y, Hu D, et al. ACS. Appl. Mater. Inter. 2017;9:34078-84.
30. Oliveira CA, Longo E, Varela JA, Zaghete MA. Synthesis and characterization of lead zirconate titanate (PZT) obtained by two chemical methods. Ceram Int. 2014;40:1717-22.